Title: **Comparative Assessment on Irreversible Losses in Heat Pumps using R744/R32/R1234yf and R744/R32/R1234ze(E)**

ABSTRACT

This paper presents an experimental assessment of COP and irreversible loss in the heat pump cycle using HFO base ternary mixtures: YF300 (R744/R32/R1234yf; 4/44/52 mass%), YF200 (R744/R32/R1234yf; 5/28/67 mass%), ZE300 (R744/R32/R1234ze(E); 4/43/53 mass%), and ZE200 (R744/R32/R1234ze(E); 9/29/62 mass%). The smaller volumetric capacity of YF200 and ZE200 increases the irreversible loss caused by the pressure drop with increasing heat load. ZE200, which has a temperature glide of approximately 22 K, increases the irreversible loss in the condenser, evaporator, and expansion valve. The experimental results indicate that YF300 and ZE300 could be potential alternatives to R410A and R32.

NUMENCLATURES

COP	:coefficient of performance	[-]
ΔT_{glide}	:temperature glide	[K]
Q	:heat load /heat transfer rate	[W]
m	:mass flow rate	[kgs^{-1}]
h	:specific enthalpy	[Jkg^{-1}]
h'	:specific enthalpy assuming isentropic process	[Jkg^{-1}]
W	:work	[W]
W'	:work assuming isentropic process	[W]
s	:specific entropy	[$Jkg^{-1}K^{-1}$]
L	:irreversible loss per unit mass	[Jkg^{-1}]
T	:temperature	[K]
P	:pressure	[Pa]

η	:compressor efficiency	[-]
η_{II}	:exergy efficiency	[-]
ρ	:density	[kgm^{-3}]
VC	:volumetric capacity	[Jm^{-3}]

superscript

n	:number of segment

subscripts

actual	:actual cycle
bub	:bubble point
COMPR	:compressor
COND	:condenser
crit	:the critical state
dew	:dew point
EVA	:evaporator
EXP	:expansion valve
H	:heat loss
H2O	:water
ideal	:ideal cycle with no pressure drop
in	:inlet
LV	:latent heat of evaporation
out	:outlet
P	:pressure drop
ref	:refrigerant
rev	:reversible cycle
s	:isentropic process
total	:total

INTRODUCTION

For environmental conservation, selecting low GWP (global warming potential) refrigerants for air-conditioning systems is one of the most important international tasks. In the past decade, several studies related to new refrigerants, namely, hydro-fluoro-olefins (HFOs), have been reported. For instance, Brown et al. (2010) predicted

the thermodynamic properties of eight HFOs: R1225ye(E), R1225ye(Z), R1225zc, R1234ye(E), R1234yf, R1234ze(E), R1234ze(Z), and R1243zf. These HFOs also emerged as candidates in a comprehensive screening by McLinden *et al*. (2014). Among them, commercialized HFOs R1234yf and R1234ze(E), with GWP less than 1 (Myhre *et al*., 2013), were considered the most promising candidates. However, the research revealed that R1234yf and R1234ze(E) exhibit considerably lower COP (coefficient of performance) or require significantly larger unit bodies at a certain rating cooling/heating load relative to the conventional refrigerant R410A. This difference is due to their smaller volumetric capacities, which require a greater volumetric flow rate to maintain the cooling/heating load, resulting in further irreversible loss.

As the second attempt, HFO-based refrigerant mixtures were developed as R410 replacements (e.g., Wang and Amrane, 2014). Table 1 shows the HFO base mixtures recently assigned by ASHRAE (ASHRAE SSPC34, 2015). As listed in Table 1, seven of the 12 mixtures contain R32 (GWP_{100} = 677), which exhibits relatively large volumetric capacity. Koyama *et al.*, (2010, 2011) selected R32 as the other component of the R1234ze(E)-based binary mixture and performed a drop-in experiment with a 2.2 kW class heat pump cycle. It was found that R1234ze(E)/R32 is a potential replacement for R410A with soft optimization of the mechanical elements. Okazaki *et al*., (2010) and Hara *et al*., (2010) examined R32/R1234yf in their products, 2.0 kW class direct expansion type air-conditioners developed for R410A, and compared COP at a rating condition. They concluded that the mass fraction of R1234yf needs to be greater than 50% to maintain the same COP as of R410A.

In this study, R744 is added into R32/R1234yf and R32/R1234ze(E) to improve their volumetric capacity. The

mixtures of R744/R32/R1234yf and R744/R32/R1234ze(E) are zeotropes; thus, temperature glide is encountered during condensation and evaporation. When the temperature glide matches the temperature change of the heat sink and source, the irreversible losses in the heat exchangers are minimized (e.g., Jakobs and Kruse, 1978, Kruse, 1981, McLinden and Radermacher, 1987, Swinney *et al*., 1998). The boiling and condensation heat transfer coefficient is drastically decreased by the mass transfer resistance in these zeotropic refrigerant mixtures (Wang *et al*., 2012; Kondou *et al*., 2015). To understand the feasibility of the selected mixtures as low-GWP alternatives for residential or commercial heat pump systems, the relation between the COP and cooling/heating load, the irreversible loss in each element, and the temperature distribution are discussed based on the experimental data.

EXPERIMENTAL METHOD

Experimental Apparatus

Figure 1 shows the experimental apparatus used for the drop-in experiments. The apparatus consists of a refrigerant loop, a heat sink water loop, and a heat source water loop. The refrigerant loop is composed of an inverter-controlled hermetic-type compressor, an oil separator, two double-tube-type heat exchangers in a counter flow configuration as the condenser and the evaporator, a liquid receiver, and a solenoid expansion valve. The refrigerant mass flow rate is measured at the liquid line between the condenser and the expansion valve by a Coriolis mass flow meter with an accuracy of 0.6 kg s^{-1}. The input powers to the compressor and inverter module are measured by a digital power meter with an accuracy of 0.1 W. For the in-situ measurement of the refrigerant mass fraction, a sampling port is connected to the liquid line. At this sampling port, the circulation liquid of

approximately 1 cm^3 is instantaneously sampled in a small chamber, and a completely vaporized refrigerant sample is assayed by a TCD (thermal conductivity detector) gas chromatograph with an accuracy of 1 mass%. From constant-temperature baths, heat sink water and heat source water controlled at certain temperatures and flow rates are supplied to the condenser and the evaporator, respectively. In mixing chambers installed between the above elements in the refrigerant loop, the pressure and bulk mean temperature are measured with accuracies of ± 7 kPa for the high-pressure side, ± 3.8 kPa for the low-pressure side, and ±0.05 K to calculate the refrigerant state with REFPROP 9.1 (Lemmon *et al*., 2013). All of the equations of state and the interaction parameters are optimized to fit the data reported in the literatures for the selected mixtures (e.g., Akasaka, 2013). In the other four mixing chambers installed in the water loops, the bulk mean water temperature at the inlet and outlet of the condenser/evaporator are measured to determine the cooling/heating loads and temperature changes of the heat sink/source.

Experimental Conditions

Table 2 lists the test refrigerants and their properties: GWP of a 100 year time horizon, normal boiling point, temperature glide at an average temperature of 293.15 K, and volumetric capacity defined as the product of latent heat and saturated vapor density. The compositions of the HFO base ternary mixtures R744/32/1234yf and R744/32/1234ze(E) are determined from the criteria at GWP_{100} of 200 and 300, and the temperature glide is less than 20 K. Compared to ZE300 and ZE200, the addition of R744 decreases GWP_{100} but increases temperature glide ΔT_{glide}. Compared to YF300 and ZE300, the R1234yf base mixture exhibits approximately 6.0 K and 9.5 K smaller

temperature glide than that of the R1234ze(E) base mixture at GWPs of 300 and 200, respectively. The volumetric capacity of the R1234yf base mixture YF300 is 1.0 MJm^{-3} larger than the R1234ze(E) base mixture ZE300 at GWP of 300. At GWP of 200, YF200 has almost comparable volumetric capacity to ZE200. Among these ternary mixtures, YF300 exhibits the smallest temperature glide and the largest volumetric capacity. The volumetric capacity of YF300 is 93% that of the conventional refrigerant R410A at 293.15 K. More specifically, the variation in the temperature glide and the volumetric capacity against the average temperature are plotted in Figure 2 for the listed test refrigerants.

Table 3 lists the experimental conditions of the heating and cooling modes performed for air-conditioning applications. Over the entire range of test conditions, the degree of superheat at the evaporator outlet is kept at 3 K. For the heating mode, the heat sink water temperatures at the inlet and outlet of the condenser are kept at 293.15 K and 318.15 K, respectively. The heat source water temperatures at the inlet and outlet of the evaporator are kept at 288.15 K and 282.15 K. The heating load is varied from 1.6 kW to 2.6 kW by adjusting the water flow rates. Similarly, for the cooling mode, the heat sink water temperature changes from 303.15 K to 318.15 K in the condenser, and the heat source water temperature changes from 293.15 K to 283.15 K in the evaporator. Then, the cooling load is varied from 1.4 kW to 2.4 kW by adjusting the water flow rate.

The amount of refrigerant charge is also varied as one of the experimental parameters to maintain the pressure ratio of the compressor discharge to suction below 6. Then, the optimum charge amount that maximizes the COP is

found. With the optimum charge amount, the degree of subcooling of the refrigerants typically ranges from 5 K to 25 K. The isentropic efficiency of the compressor ranges from 0.82 to 0.93. The heat losses in the discharge line, including the oil separator, the connection line between the condenser and expansion valve, and the suction line, range from 0.09 to 0.12 kW and are taken into account in the evaluation of irreversible loss. In addition, the pressure loss in the suction line around the compressor is considerably large and is necessarily taken into account in the loss analysis.

Data Reduction

The cooling and heating loads, namely, the heat transfer rates in the condenser and evaporator, are calculated from the refrigerant-side heat balance, as follows:

$$Q_{\mathrm{COND}} = m_{\mathrm{ref}} \left(h_{\mathrm{COND,in}} - h_{\mathrm{COND,out}} \right) \tag{1}$$

$$Q_{\mathrm{EVA}} = m_{\mathrm{ref}} \left(h_{\mathrm{EVA,out}} - h_{\mathrm{EVA,in}} \right) \tag{2}$$

where Q is the heat transfer rate, m_{ref} is the mass flow rate of the refrigerant, and h is the specific enthalpy. The subscripts COND and EVA indicate the condenser and the evaporator, respectively. The subscripts “in” and “out” indicate the inlet and the outlet, respectively. The propagated measurement uncertainties in the heat transfer rates Q_{COND} and Q_{EVA} are 1.5 and 2.5%, respectively. These heat transfer fates obtained from the refrigerant-side heat balance agree with those of the water-side heat balance within 1.0%.

The cooling and heating COPs are obtained from the above heat load and the compression work, W_{COMPR}, which is found from the specific enthalpy difference between the compressor suction and discharge.

$$COP_{\mathrm{COND}} = \frac{Q_{\mathrm{COND}}}{W_{\mathrm{COMPR}}} = \frac{h_{\mathrm{COND,in}} - h_{\mathrm{COND,out}}}{h_{\mathrm{COMPR,out}} - h_{\mathrm{COMPR,in}}} \tag{3}$$

$$COP_{\mathrm{EVA}} = \frac{Q_{\mathrm{EVA}}}{W_{\mathrm{COMPR}}} = \frac{h_{\mathrm{EVA,out}} - h_{\mathrm{EVA,in}}}{h_{\mathrm{COMPR,out}} - h_{\mathrm{COMPR,in}}} \tag{4}$$

These COPs take into account the compressor isentropic efficiency, but not the mechanical, volumetric, and inverter efficiencies. The propagated measurement uncertainty in the COP was within 5%. The compressor isentropic efficiency is defined as

$$\eta_{\mathrm{s}} = \frac{W'_{\mathrm{COMPR}}}{W_{\mathrm{COMPR}}} = \frac{h'_{\mathrm{COMPR,out}} - h_{\mathrm{COMPR,in}}}{h_{\mathrm{COMPR,out}} - h_{\mathrm{COMPR,in}}} \tag{5}$$

where $h'_{\mathrm{COMPR,out}}$ is the ideal compressor discharge specific enthalpy on the isentropic curve departing from the point that refers to the compressor suction.

$$h'_{\mathrm{COMPR,out}} = f\left(P_{\mathrm{COMPR,out}}, s_{\mathrm{COMPR,in}}\right) \tag{6}$$

For the performance assessment of heat pump cycles, the irreversible loss (de'Rossi *et al.*, 1991) is calculated as follows. The total irreversible loss during cycling, L_{total}, can be divided into the following irreversible losses of the main elements (e.g., compressor and evaporator) and also the heat loss and pressure drop, as follows:

$$L_{\mathrm{total}} = L_{\mathrm{COND}} + L_{\mathrm{EVA}} + L_{\mathrm{EXP}} + L_{\mathrm{COMPR}} + L_{\mathrm{H}} + L_{\mathrm{P}} \tag{7}$$

Figure 3 (a) illustrates the irreversible losses per unit refrigerant mass, L, generated in the main elements: the condenser, the evaporator, the expansion valve, and the compressor. The state of refrigerant, shown with the circle symbols, is calculated from the measured data in the mixing chambers, as shown in Figure 1. The water temperatures corresponding to the refrigerant state are also plotted on the *T-s* diagram with dashed lines, approximating that the water temperature changes proportionally with the refrigerant specific enthalpy change.

When the heat transfer coefficient is infinitely high, the refrigerant temperature asymptotically approaches the water temperature, and irreversible loss is minimized. Therefore, the irreversible loss in the condenser and evaporator is represented by area "9-13-14-10" of L_{COND} and area "11-15-8-12" of L_{EVA}, as shown in Figure 3 (a). These areas are equally partitioned into 100 segments in the direction of the entropy and are quantified as follows:

$$L_{\mathrm{COND}} = \sum_{n}\left[\left(T_{\mathrm{ref}}^{n} - T_{\mathrm{H2O}}^{n}\right) + \left(T_{\mathrm{ref}}^{n+1} - T_{\mathrm{H2O}}^{n+1}\right)\right]\Delta s^{n} / 2 \tag{8}$$

$$L_{\mathrm{EVA}} = \sum_{n}\left[\left(T_{\mathrm{H2O}}^{n} - T_{\mathrm{ref}}^{n}\right) + \left(T_{\mathrm{H2O}}^{n+1} - T_{\mathrm{ref}}^{n+1}\right)\right]\Delta s^{n} / 2 \tag{9}$$

where T_{ref} and T_{H2O} are the temperatures of the refrigerant and water, respectively, and Δs is the specific entropy change through a segment, as illustrated in Figure 3 (a). The irreversible losses generated in the compressor and the expansion valves are represented by area "1-2-3-4" of L_{COMPR} and area "5-6-7-8" of L_{EXP}, as shown in Figure 3 (a).

$$L_{\mathrm{COMPR}} = \left(T_{\mathrm{COMPRin}} + T_{\mathrm{COMPRout}}\right)\left(s_{\mathrm{COMPRout}} - s_{\mathrm{COMPRin}}\right) / 2 \tag{10}$$

$$L_{\mathrm{EXP}} = \left(T_{\mathrm{EXPin}} + T_{\mathrm{EXPout}}\right)\left(s_{\mathrm{EXPout}} - s_{\mathrm{EXPin}}\right) / 2 \tag{11}$$

When the compressor isentropic efficiency approaches 1.0, the former irreversible loss L_{COMPR} is asymptotic to 0. The latter irreversible loss L_{EXP} is obtained with an assumption of an isenthalpic process. Additionally, the hatched areas "1-9-10-11-12-2" and "13-5-8-15-14" of L_{H} represent the irreversible loss caused by heat loss in the discharge line between the compressor and the condenser, the liquid line between the condenser and the expansion valve, and the suction line between the evaporator and the compressor.

Figure 3 (b) illustrates the irreversible loss caused by the pressure drop L_{P}. The pressure drop during the condensation and evaporation is assumed to be proportional to the specific enthalpy change. This irreversible loss L_{P} is obtained as the difference of the actual cycle from the ideal cycle, assuming no pressure drop. In Figure 3 (b),

the dashed line shows the ideal cycle obtained from only the specific enthalpy change, eliminating the effect of the pressure drop. The evaporation side of pressure drop, the hatched area "EVA, side", is considered to be negative.

$$L_{\mathrm{P}} = \sum_{n} \left[\left(s_{\mathrm{ref}}^{n+1} - s_{\mathrm{ref,ideal}}^{n} \right) \left(T_{\mathrm{ref}}^{n} - T_{\mathrm{ref,ideal}}^{n+1} \right) + \left(s_{\mathrm{ref}}^{n} - s_{\mathrm{ref,ideal}}^{n+1} \right) \left(T_{\mathrm{ref,ideal}}^{n} - T_{\mathrm{ref}}^{n+1} \right) \right] / 2 \tag{12}$$

If the other irreversible losses were negligible, the compression work in Eqs. (3) and (4) is also described by the heat balance in this corollary of the tested heat pump system:

$$W_{\mathrm{COMPR}} + Q_{\mathrm{EVA}} \approx Q_{\mathrm{COND}} + L_{\mathrm{total}} m_{\mathrm{ref}} \tag{13}$$

$$\therefore W_{\mathrm{COMPR}} \approx Q_{\mathrm{COND}} + L_{\mathrm{total}} m_{\mathrm{ref}} - Q_{\mathrm{EVA}} \tag{14}$$

The right hand side in the above equation agrees with the measured compressor work W_{COMPR} within 0.2%. From this confirmation, the assumption and approximations in the pressure and water temperature distribution in the condenser and evaporator was justified as an adequately accurate analysis of the irreversible losses.

Figure 4 depicts an exergy and anergy (i.e., enthalpy) flow model (Rant, 1956) of the tested heat pump system described in Eq. (13). The irreversible loss mentioned above represents the exergy destruction. When that irreversible loss eventuate to zero, the input work is ultimately minimized in a reversible cycle. Thus, an exergy efficiency, which is also called as second law efficiency, is defined as a ratio of input exergy to output exergy. Often this efficiency is expressed as a ratio of work used in actual cycle to that of in a reversible cycle (Bejan, 1988) for heat pump systems.

$$\eta_{\mathrm{II}} = \frac{W_{\mathrm{rev}}}{W_{\mathrm{actual}}} = \frac{\left(W_{\mathrm{COMPR}} - L_{\mathrm{total}} m_{\mathrm{ref}} \right)}{W_{\mathrm{COMPR}}} \tag{15}$$

The work of reversible cycle per unit mass flow rate ($W_{\mathrm{rev}}/m_{\mathrm{ref}}$) is shown as the center area of Figure 3 (a). The above exergy efficiency can be transcribed with COP as,

$$\eta_{II} = \begin{cases} \dfrac{\left(Q_{EVA}/W_{actual}\right)}{\left(Q_{EVA}/W_{rev}\right)} = \dfrac{\left(COP_{EVA}\right)_{rev}}{\left(COP_{EVA}\right)_{actual}} = \dfrac{\left[Q_{EVA}/\left(W_{COMPR} - L_{total}m_{ref}\right)\right]}{\left(COP_{EVA}\right)_{actual}} & \text{for cooling mode} \\ \dfrac{\left(Q_{COND}/W_{actual}\right)}{\left(Q_{COND}/W_{rev}\right)} = \dfrac{\left(COP_{COND}\right)_{rev}}{\left(COP_{COND}\right)_{actual}} = \dfrac{\left[Q_{COND}/\left(W_{COMPR} - L_{total}m_{ref}\right)\right]}{\left(COP_{COND}\right)_{actual}} & \text{for heating mode} \end{cases} \quad (16)$$

EXPERIMENTAL RESULTS

COP and Exergy Efficiency

Figures 5 (a) and (b) show the experimentally evaluated cooling and heating COP, respectively, at various cooling/heating loads with optimization of the refrigerant charge. Because of the limitation of the compressor operation range, no data were taken for R410A and R32 at heat loads below 1.8 kW. At heat loads of below 1.8 kW, ZE300 exhibits the highest COP for both operation modes; however, the COP drastically decreases with increasing heat loads. This trend is more obvious in the COP of ZE300, ZE200, and YF200. Thus, at heat loads above 2.2 kW, R32 exhibits the highest COP followed by R410A and ZE300. At a cooling load of 2.0 kW and a heating load of 2.2 kW, which are the rating conditions of the experimental apparatus, the COPs of ZE300 and YF300 are comparable to R410A but are somewhat lower than R32, which indicates that ZE300 and YF300 could replace R410A with drop-in. As the replacement of R32, the materials require soft optimization of the mechanical element, for instance, larger tube diameter and compressor displacement volume.

Figures 6 (a) and (b) show the exergy efficiency obtained from Eq. (15) at various cooling/heating loads. The exergy efficiency ranges from 0.35 to 0.46 for cooling mode, and from 0.34 to 0.0.43 for heating mode. Under a given temperature condition of heat source and heat sink fluids, the reversible work per unit refrigerant flow rate

(W_{rev}/m_{ref}), illustrated in Figure 3, is unambiguously determined. Consequently, the general tendency of the exergy efficiency against the heat load is very similar to that of COP as plotted in Figure 5. Because the average temperature difference between source fluid and sink fluid of cooling mode is larger than that of heating mode, the unit reversible work (W_{rev}/m_{ref}) of cooling mode is greater than that of heating mode. This results the higher exergy efficiency of cooling mode than the heating mode. As the heat load increases, the refrigerant mass flow rate and the irreversible losses, namely the exergy destruction, are increased. Thus, the exergy efficiency decreases with increasing heat load. As discussed above, the irreversible loss dominates the exergy efficiency and also the COP. To increase the exergy efficiency and COP, the irreversible losses generated in the actual cycle have to be reduced.

Breakdown of the Irreversible Loss

Figures 7 (a) and (b) compare the breakdown of the irreversible loss between the test refrigerants at a cooling load of 2.0 kW and a heating load of 2.2 kW, respectively, for the attribution analysis of COP. A smaller irreversible loss in total, indicates higher COP, as described in Eq. (14). Thus, R32 exhibits the smallest irreversible loss among the test refrigerants followed by ZE300, R410, and YF300.

At a cooling load of 2.0 kW, for instance, the average of irreversible loss of the tested refrigerants in each attribution are as follows. The irreversible loss during the compression process is approximately 33% of the total loss. The losses in the condenser, evaporator, and expansion valve are 25%, 17%, and 16% of the total, respectively. The losses caused by pressure drop and heat loss are 6% and 3%. At a heating load of 2.2 kW, the average irreversible losses in compressor L_{COMPR} and condenser L_{COND} individually occupy more than 30% of the total

irreversible loss. The losses in the evaporator and expansion valve are approximately 15% and 11% of the total. The loss caused by the pressure drop and heat loss are, respectively, 6% and 3% of the total. The loss in the evaporator and expansion valve make up larger portions of the total under the cooling mode. The loss in condenser makes up a larger portion of the total loss under the heating mode. Except for the loss of the pressure drop, the irreversible loss of the tested refrigerant increases with increasing heat load at the same attribution ratio. Only the loss of the pressure drop has a significantly different increment ratio between refrigerants. Although the portion of pressure drop is relatively small in the total loss, the difference in the increment ratio of loss caused by the pressure drop dominantly differs with the variation in COP against heat loads, as shown in Figure 5.

Irreversible Loss Caused by the Pressure Drop

Figure 8 shows the variation in the irreversible loss caused by the pressure loss against the heating load. For all of the test refrigerants, the irreversible loss of pressure drop monotonically increases with increasing heat load. However, the rate of increment depends on the refrigerant. The ratios of ZE300, ZE200, and YF200 are more than twice that of R410. On the other hand, the ratio of R32 is approximately 70% that of R410A. This tendency is related to the volumetric capacity listed in Table 2. The ZE200, ZE300, and YF200, which have smaller volumetric capacity, increase the refrigerant volumetric flow rate more than the other refrigerants, and the momentum is more dissipated in the cycle. To reduce this pressure drop, a larger tube diameter and branch of refrigerant circuit in the heat exchangers are needed. From the viewpoint of pressure drop reduction, YF300 is more favorable than ZE300, ZE200, and YF200.

Irreversible Loss in Heat Exchangers

As shown in Figure 7, among the tested refrigerants, ZE300 exhibits the smallest loss in condenser L_{COND} at a cooling load of 2.0 kW, which can be explained by the temperature difference between the refrigerant and heat source. Figure 9 shows the temperature distribution of the refrigerant and heat source/sink in the condenser and evaporator at the rating heat loads. ZE300, with a temperature glide of 13.7 K at an average saturation temperature of 293.15 K, matches the heat sink temperature change in the condenser of 15 K, which reduces the overall temperature difference between the refrigerant and heat sink. On the other hand, R32 and R410A have a pinch point at the dew point, which enlarges the temperature difference in the subcooling region near the bubble point. Regarding the irreversible loss in evaporator L_{EVA}, YF300, which has the smallest temperature glide, exhibits the smallest loss and temperature difference during the evaporation process, as plotted in Figure 9, because the temperature change of the heat source in the evaporator is smaller than that of the heat sink.

According to the concept of the Lorenz cycle, ideally, the approaching temperature difference and the irreversible loss in heat exchangers can be minimized when the temperature glide of the zeotropic mixtures matches the temperature changes of the heat sink and source. However, in a real cycle involving the de-superheating and subcooling regions, to achieve such ideal utilization of temperature glide is difficult and unfortunately unrewarding for various operation conditions, especially for air conditioning applications. Nevertheless, the summation of the losses in the evaporator and condenser of YF300, ZE300, and YF200 are comparable or slightly smaller than those of R32 and R410A. ZE300, which has a temperature glide of more than 20 K, has the largest irreversible loss, L_{EVA}

+ L_{COND}. For the tested conditions, the mixtures with temperature glides more than 20 K increase the irreversible loss in the condenser and evaporator.

Irreversible Loss in the Expansion Valve

As shown in Figure 7, the irreversible losses in the expansion valve of R32 and R410A are smaller than the tested HFO base refrigerant mixture. R32 and R410A have significantly large subcooling at the inlet of the expansion valve, as shown in Figure 9, accordingly a smaller vapor quality at the outlet, which reduces the momentum dissipation and entropy generation during the expansion process. Because the tested HFO base mixtures have temperature glide, the subcooling at the inlet of the expansion valve is relatively smaller than that of R32 and R410. Thus, the tested HFO mixtures generate larger irreversible losses during the expansion process. The summations of L_{COND}, L_{EVA}, and L_{EXP} for YF300 and ZE300 are comparable to R32 and R410A, which indicates these two mixtures are potential alternatives to R32 and R410A with optimization of the mechanical elements.

Irreversible Loss in the Compressor

With the combination of the tested compressor and lubricant oil POE-VG68, ZE300 exhibits the smallest irreversible loss in the compressor. This result was unexpected because a small volumetric capacity increases compressor rotation speed and reduces compressor efficiency. The rotation speed of the compressor and solubility of the oil was favorable for ZE300. By selecting the compressor size and lubricant oil, this irreversible loss can be reduced. To determine the best combination, further study of the compressor efficiency curve, the solubility of the

lubricant oil, and their effect of the isentropic efficiency is needed.

CONCLUSIONS

R1234yf-based refrigerant mixtures YF300 (R744/R32/R1234yf; 4/44/52 mass%) and YF200 (R744/R32/R1234yf; 5/28/67 mass%) and R1234ze(E)-based refrigerant mixtures ZE300 (R744/R32/R1234ze(E); 4/43/53 mass%) and ZE200 (R744/R32/R1234ze(E); 9/29/62 mass%) were examined with a 2.0-kW class heat pump cycle. The COP and irreversible losses of the mixtures are compared to those of R410A and R32. The smaller volumetric capacity of YF200 and ZE200 significantly increases the irreversible loss caused by the pressure drop as the heat load increases. Consequently, the COPs of YF200 and ZE200 are lower than those of R410A and R32 at the rating heat load. ZE200, which has a temperature glide of approximately 22 K, increases the irreversible loss in the condenser, evaporator, and expansion valve. A temperature glide of more than 20 K is challenging for air-conditioning applications. Overall, the experimental results indicate that YF300 and ZE300 are potential alternatives to R410A and R32.

REFERENCES

ASHRAE agenda-ttachment4-2015 IMC code change proposal SSPC34 meeting 24 January 2015- Chicago, IL, draft1.

Akasaka, R., 2013. Thermodynamic property models for the difluoromethane (R-32) + trans-1,3,3,3-tetrafluoropropene (R-1234ze(E)) and difluoromethane + 2,3,3,3-tetrafluoropropene (R-1234yf) mixtures. *Fluid Phase Equilib*. 358, 98–104.

Bejan, A., 1988. Advanced Engineering Thermodynamics, Wiley-Interscience Publication, NY, USA, 111-140.

Brown, J.S., Zilio, C., Cavallini, A., 2010. Thermodynamic properties of eight fluorinated olefins. *Int. J. Refrig*. 33, 235–241.

de'Rossi, F., Mastrullo, R., Mazzei, P., 1991. Working fluids thermodynamic behavior for vapor compression

cycles. *Appl. Energy*, 38, 163–180.

Hara, H., Oono, M., Iwata, I., Experimental Study of Low GWP Refrigerants for Room Air-Conditioners, 2010 International Symposium on Next-generation Air Conditioning and Refrigeration Technology, Tokyo, Japan, 2010.

Jakobs, R., Kruse, H., 1979. The use of non-azeotropic refrigerant mixtures in heat pumps for energy saving, *Int. J. Refrig.* 4 (3) 119-125.

Kondou, C., Mishima, F., Koyama, S., 2015. Condensation and evaporation of R32/R1234ze(E) and R744/R32/R1234ze(E) flow in horizontal microfin tubes. *Sci. Technol. Built Environ*. 21, 564–577.

Koyama, S., Matsuo, Y., Fukuda S., Akasaka, R. 2010a, Measurement of vapor-liquid equilibrium of HFO1234ze(E) / HFC-32, *Proc. 2010 JSRAE Annual Conference*, 195-196.

Koyama, S., Takata, N., Fukuda, S. 2010b, Drop-in experiments on heat pump cycle using HFO-1234ze(E) and its mixtures with HFC-32, *Proc. Int. Refrig. A/C Conf. at Purdue*, Paper no. 2514, 1-8.

Kruse, H., The advantages of non-azeotropic refrigerant mixtures for heat pump application, *Int. J. Refrig.* 4(3):119-125, 1981

Lemmon E.W., Huber M.L., McLinden M.O., 2013. Reference Fluid Thermodynamic and Transport Properties - REFPROP Ver. 9.1. National Institute of Standards and Technology, Boulder, CO, USA.

McLinden, M.O., Kazakov, A.F., Steven Brown, J., Domanski, P., 2014. A thermodynamic analysis of refrigerants: Possibilities and tradeoffs for Low-GWP refrigerants. *Int. J. Refrig*. 38, 80–92. doi:10.1016/j.ijrefrig.2013.09.032

McLinden, M.O., Radermacher, R., 1987. Methods for comparing the performance of pure and mixed refrigerants in the vapour compression cycle, *Int. J. Refrig.* 10 (6) 318-325.

Myhre, G., Shindell, D., Bréon, F.-M., Collins, W., Fuglestvedt, J., Huang, J., Koch, D., Lamarque, J.F., Lee, D., Mendoza, B., Nakajima, T., Robock, A., Stephens, G., Takemura, T., Zhan, H., 2013. Anthropogenic and Natural Radiative Forcing, in: Climate Change 2013: The Physical Science Basis. Contribution of Working Group I to the Fifth Assessment Report of the Intergovernmental Panel on Climate Change.

Okazaki, T., Maeyama, H., Saito, M., Yamamoto, T., Performance and Reliability Evaluation of a Room Air Conditioner with Low GWP Refrigerant, 2010. *Proc. Int. Symp. Next-generation Air Conditioning and Refrigeration Tech.*, Tokyo, Japan.

Rant, Z., 1956. Exergy, a New Word for Technical Available Work (Exergie, ein neues Wort für ‘technische Arbeitsfähigkeit’) *Forschungen im Ingenieurwesen*, vol. 22, 36-37 (in German).

Solomon, S., Qin, D., Manning, M., Chen, Z., Marquis, M., Averyt, K.B., Tignor, M., H.L. Miller (eds.), 2007. Contribution of Working Group I to the Fourth Assessment Report of the Intergovernmental Panel on Climate Change, Cambridge University Press, Cambridge, United Kingdom and New York, NY, USA.

Swinney, J., Jones, W.E., Wilson, J.A., 1998. The impact of mixed non-azeotropic working fluids on refrigeration system performance, Int. J. Refrig., vol. 21, no. 8, 607-616.

Wang, L., Dang, C., Hihara, E., 2012. Experimental and theoretical study on condensation heat transfer of nonazeotropic refrigerant mixtures R1234yf/R32 inside a horizontal smooth tube. *Proc. Int. Refrig. Air Conditioning Conf*. Paper 1308.

Wang, X., Amrane, K., 2014. AHRI Low Global Warming Potential Alternative Refrigerants Evaluation Program (Low-GWP AREP) – Summary of Phase I Testing Results. *Proc. Int. Refrig. Air Conditioning Conf.* paper1416, 10.

Table 1 ASHRAE SSPC34 HFO-based refrigerant mixtures

designation	composition (mass%)	GWP_{100}	NBP[1)]	T_{crit}	P_{crit}	ρ_{crit}	safety [2)]	Δh_{LV}[3)]	ΔT_{glide}[3)]
		-	K	K	kPa	kgm^{-3}	-	$kJkg^{-1}$	K
R444A	R32/R152a/R1234ze(E) (12.0/5.0/83.0)	89	248.15	375.95	4361	472	A2L	197	10.2
R444B	R32/R152a/R1234ze(E) (41.5/10.0/48.5)	295	237.15	365.25	5212	444	A2L	229	8.1
R445A	R744/R134a/R1234ze(E) (6.0/9.0/85.0)	118	249.15	378.25	4529	480	A2L	203	21.5
R446A	R32/R1234ze(E)/R600(68.0/29.0/3.0)	461	228.15	357.35	5635	433	A2L	246	4.0
R447A	R32/R125/R1234ze(E) (68.0/3.5/28.5)	572	227.15	355.75	5536	442	A2L	240	3.4
R448A	R32/R125/R1234yf/R134a/R1234ze(E) (26.0/26.0/20.0/21.0/7.0)	1273	234.15	356.85	4495	480	A1	188	5.5
R449A	R32/R125/R1234yf/R134a (24.3/24.7/25.3/25.7)	1282	235.15	357.05	4387	480	A1	188	5.4
R450A	R1234ze(E)/R134a(58/42)	547	249.15	378.75	4082	499	A1	172	0.8
R451A	R1234yf/R134a(89.8/10.2)	133	244.15	368.65	3452	479	A2L	153	0.0
R451B	R1234yf/R134a(88.8/11.2)	146	244.15	368.65	3458	479	A2L	153	0.0
R452A	R32/R125/R1234yf(11.0/59.0/30.0)	1945	231.15	348.75	3911	515	A1	148	3.8
R513A	R1234yf/R134a(56.0/44.0)	573	245.15	370.85	3681	491	A1	163	0.0

1) Normal boiling point 2) ASHRAE safety classification 3) at an average temperature (T_{dew} - T_{bub})/2 of 293.15 K

Table 2 Test refrigerants

Designation	Composition (mass%)	GWP_{100}	NBP	ΔT_{glide}[1)]	VC[1)2)]
			[K]	[K]	[MJ m^{-3}]
YF300	R744/R32/R1234yf (4/44/52 mass%)	298[3)]	226.75	7.3	10.24
YF200	R744/R32/R1234yf (5/28/67 mass%)	190[3)]	230.95	11.6	9.51
ZE300	R744/R32/R1234ze(E) (4/43/53 mass%)	292[3)]	235.65	13.3	9.25
ZE200	R744/R32/R1234ze(E) (9/29/62 mass%)	197[3)]	238.35	21.1	9.56
R410A	R32/R125 (50/50mass%)	2088[4)]	221.75	0	11.06
R32	-	677[5)]	221.75	0	11.47

1) at 293.15 K 2) $VC = \Delta h_{LV} \cdot \rho_V$ 3) mass-fraction-weighted average 4) IPCC 4AR (Solomon *et al*., 2007)
5) IPCC 5AR (Myhre *et al*., 2013)

Table 3 Experimental conditions

	Cooling mode	Heating mode
Heat source temp. [K]	293.15 → 283.15	288.15 → 282.15
Heat sink temp. [K]	303.15 → 318.15	293.15 → 318.15
Degree of superheat [K]	3	
Degree of subcool [K]	determined at optimum charge	
Heat transfer rate [kW]	1.4 to 2.4	1.6 to 2.6
Refrigerant charge [g]	optimized	
Compressor displacement volume [cm^3]	11	
Lubricant oil	POE-VG68	
Compressor isentropic efficiency	0.82 to 0.93	
Inner diameter of suction tube [mm]	12.7	
Inner diameter of the other tubes [mm]	9.53	

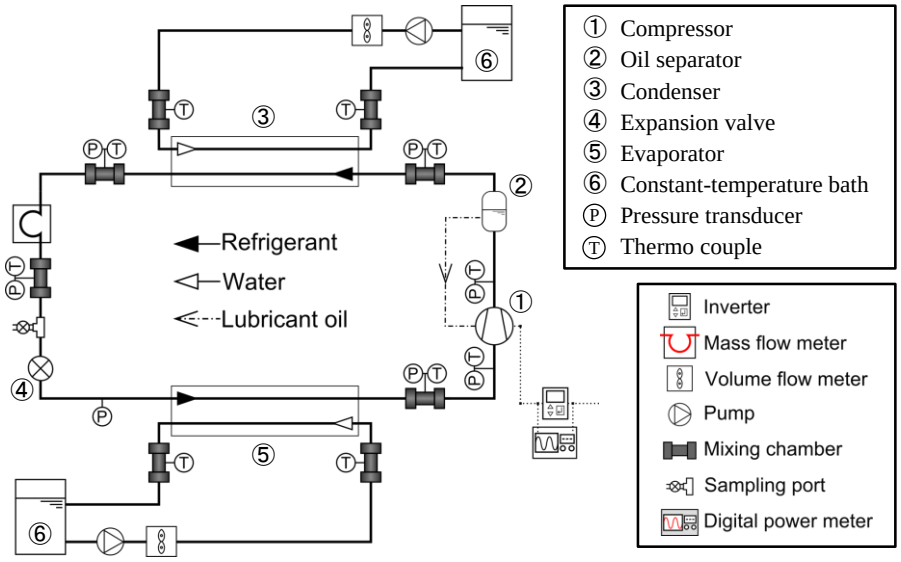

Figure 1 Experimental apparatus

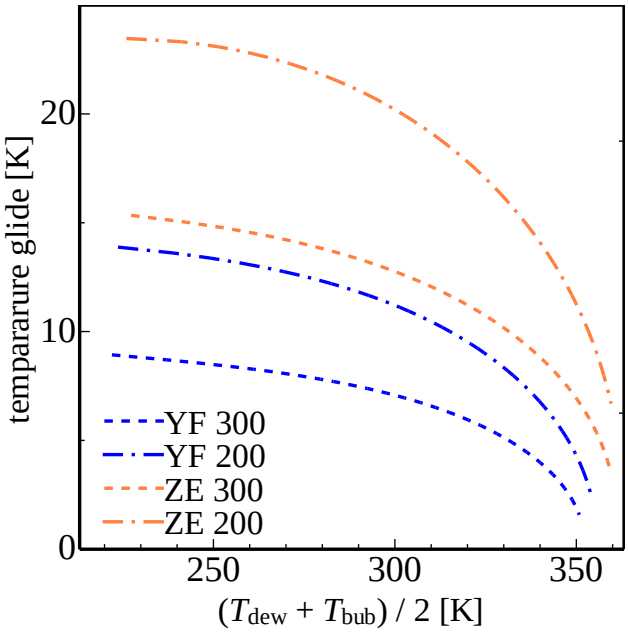

(a) temperature glide

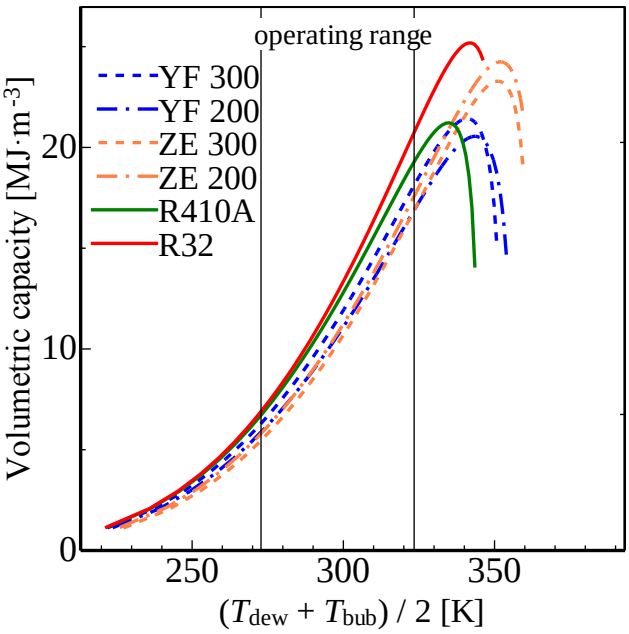

(b) volumetric capacity

Figure 2 Thermodynamic characteristics of the test refrigerants

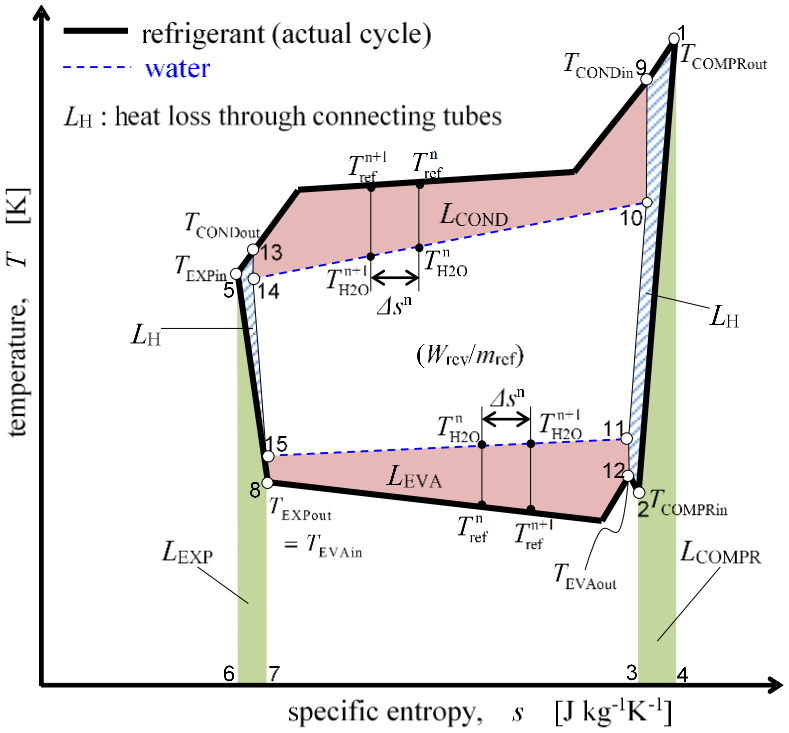

(a) loss in each element

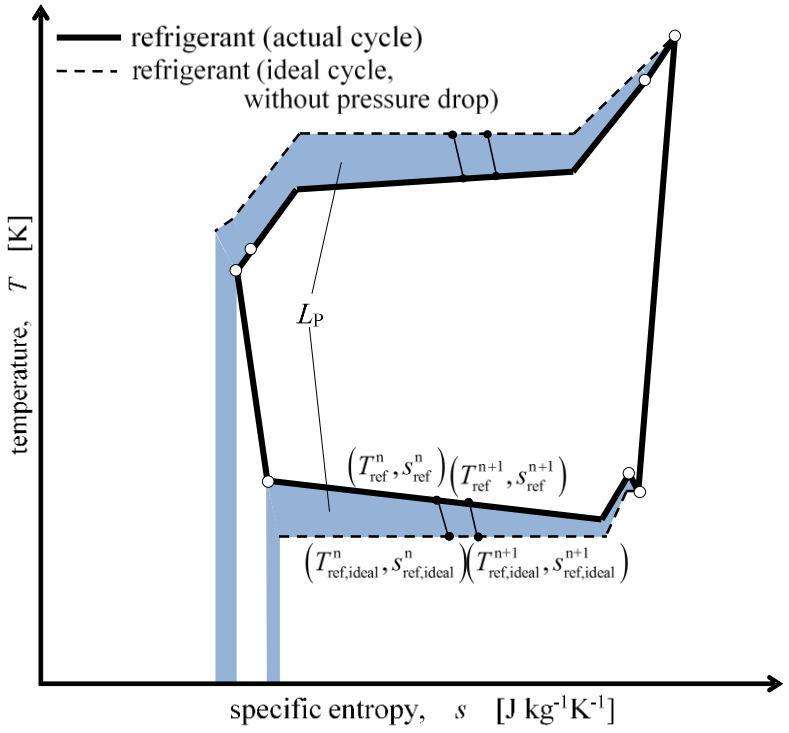

(b) loss by pressure drop

Figure 3 Methodology to calculate the irreversible losses

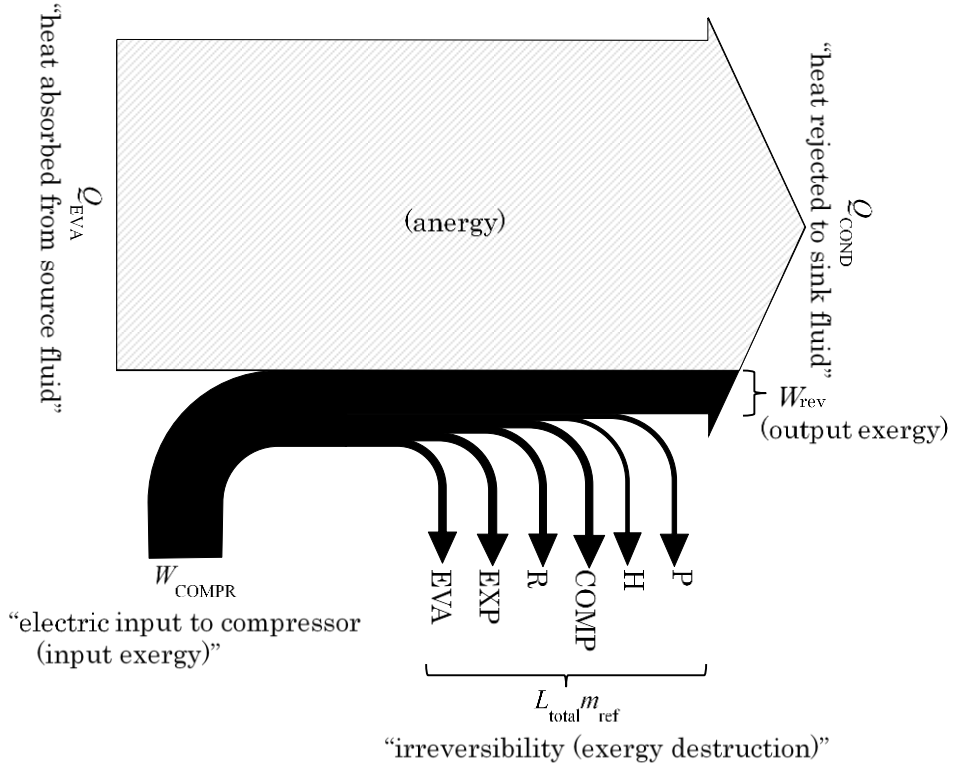

Figure 4 Model of exergy and anergy flow for the heat pump systems

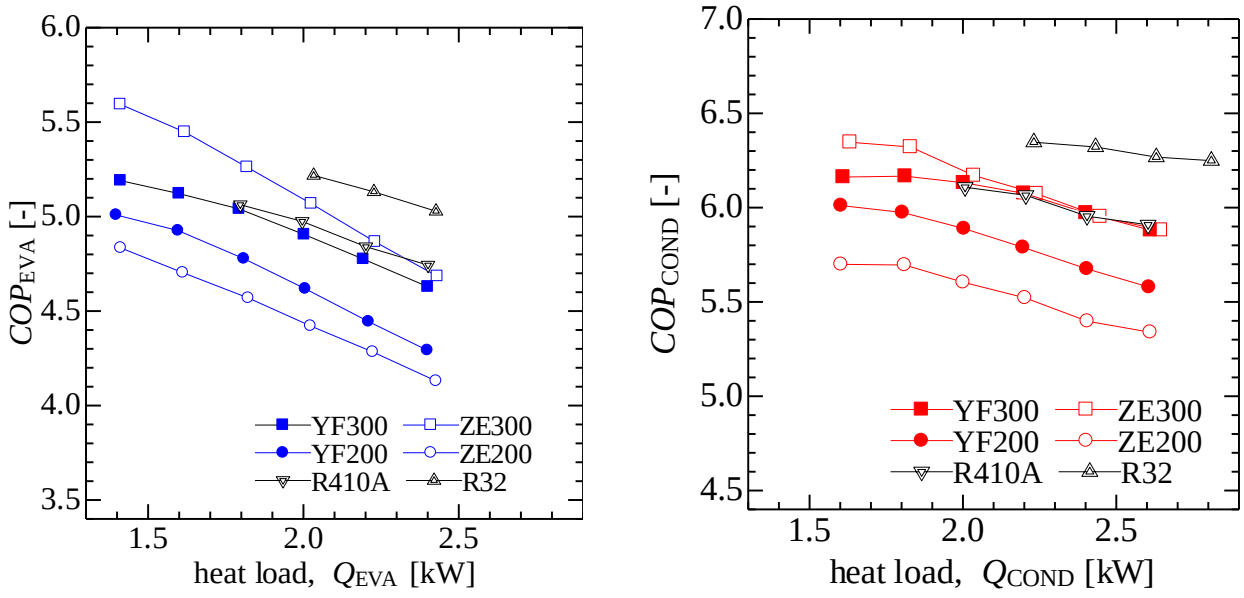

(a) cooling mode (b) heating mode

Figure 5 Comparison of the COP between test refrigerants at various heat loads

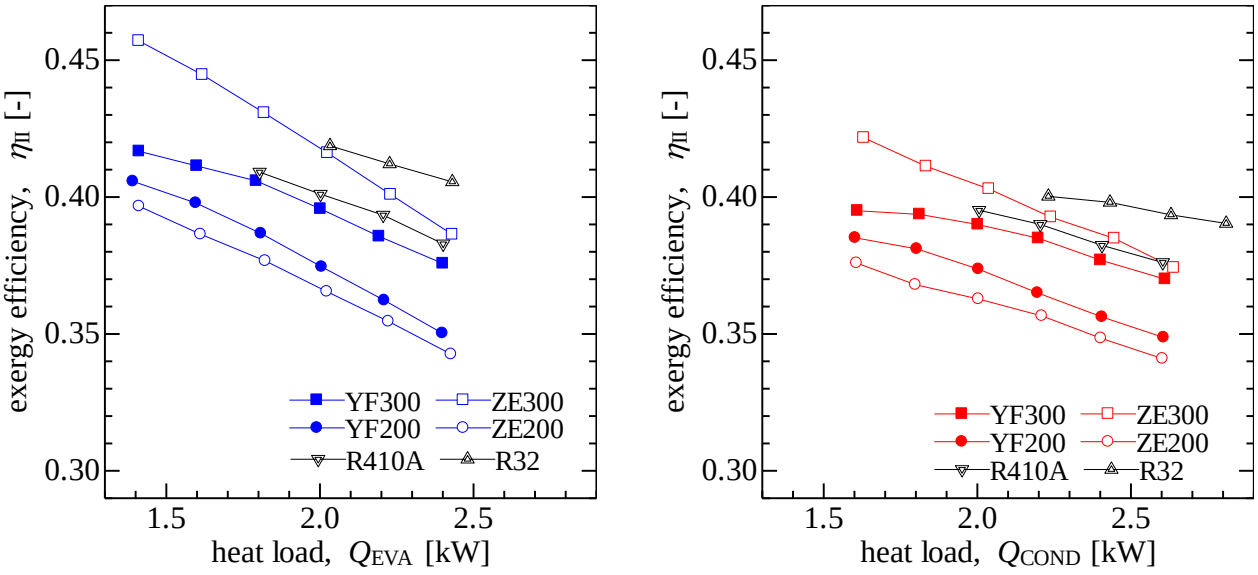

(a) cooling mode (b) heating mode

Figure 6 Comparison of the exergy efficiency between test refrigerants at various heat loads

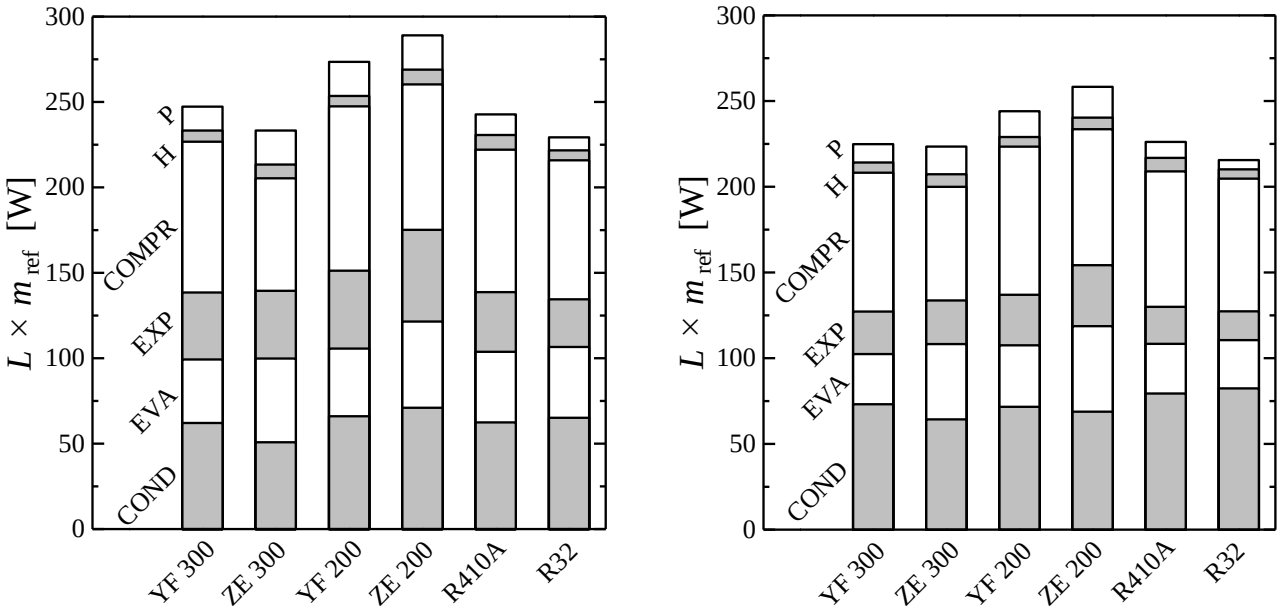

(a) at a cooling load of 2.0 kW (b) at a heating load of 2.2 kW

Figure 7 Breakdown in the irreversible loss of the test refrigerants at rating conditions

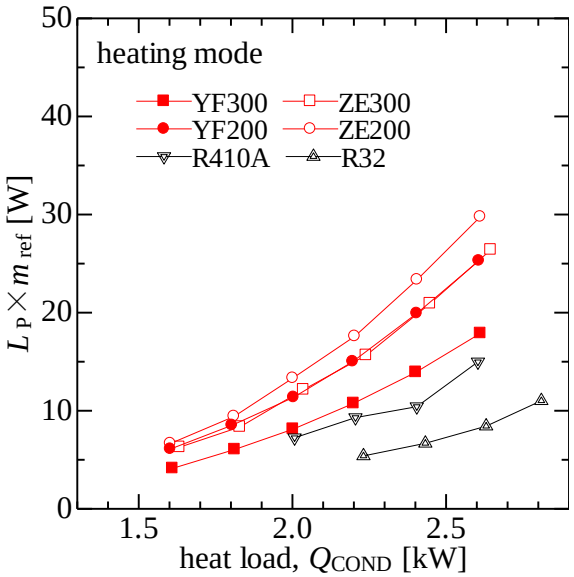

Figure 8 Comparison of the irreversible loss caused by the pressure loss for the test refrigerants

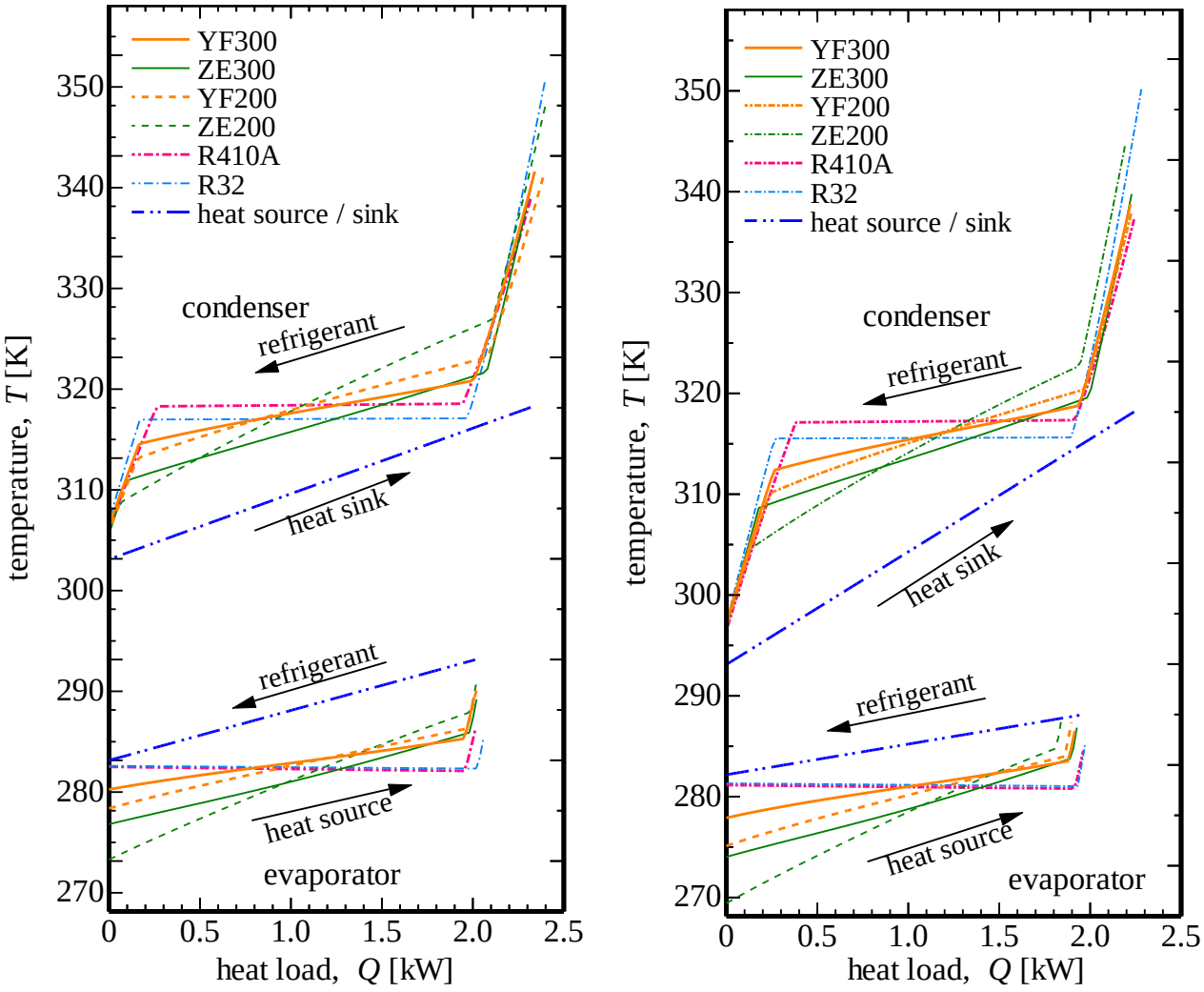

(a) at a cooling load of 2.0 kW

(b) at a heating load of 2.2 kW

Figure 9 Temperature distribution in the condenser and evaporator